A flexible multifunctional electrode based on conducting PANI/Pd composite for non-enzymatic glucose sensor and direct alcohol fuel cell

(article starts on next page)

Full Length Article

A flexible multifunctional electrode based on conducting PANI/Pd composite for non-enzymatic glucose sensor and direct alcohol fuel cell applications

Muthusankar Eswaran [a], Shadi Rahimi [a], Santosh Pandit [a], Bavatharani Chokkiah [b,c], Ivan Mijakovic [a,d,*]

[a] *Division of Systems and Synthetic Biology, Department of Biology and Biological Engineering, Chalmers University of Technology, SE-412 96 Göteborg, Sweden*
[b] *Centre for Materials Chemistry Karpagam Academy of Higher Education, Coimbatore-641046, Tamilnadu, India*
[c] *Department of Science &Humanities, Karpagam Academy of Higher Education, Coimbatore-641046, Tamilnadu, India*
[d] *Novo Nordisk Foundation Center for Biosustainability, Technical University of Denmark, DK-2800 Lyngby, Denmark*

A B S T R A C T

In this work, we fabricated a flexible, multifunctional polyimide (PI)/Au-polyaniline (PAN)/Pd nanocomposite electrode with excellent electrochemical properties. Structural geometry, morphological views, and functional group analyses indicated that the physicochemical and electrochemical performance of the electrode is based on the strong and synergistic metal-polymer interaction between the conducting PAN and Pd, which ensured high conductivity, rapid response, and high electron transfer rate through more electroactive spots available in the nanocomposite. Here, we demonstrated that the fabricated PI/Au-PAN/Pd electrodes can be successfully used for biomedical sensing of glucose, as well as for energy conversion application, using the oxidation of alcohols such as methanol and ethanol in fuel cells. The electrochemical analysis shows that the flexible sensor (PI/Au-PAN/Pd) has ultra-high sensitivity of 2140 $\mu A/\mu M.cm^2$ with a low detection limit of 0.3 μM for glucose. Also, the interference analysis, reproducibility, and stability studies reveal its excellent capability for glucose sensing. Furthermore, the electrode also demonstrates prominent electrocatalytic behavior to the electrooxidation of methanol and ethanol in an alkaline medium with a current density of 3 mA/cm^2 and 0.96 mA/cm^2 along with good cyclic stability. Thus, this efficient flexible electrocatalyst with good stability, practicability, and reproducibility claims its potential applications in flexible/wearable healthcare diagnostics systems as well as in alternative energy conversion devices.

1. Introduction

Electrocatalysis toward various small molecules with an integrated power supply system has aroused widely due to its potential applications in many technological and industrial fields including sensors/biosensors (medical, environmental, industrial sensors), energy conversion and storage devices (fuel cells, batteries, and supercapacitors), and other electrocatalytic and analytical applications. To satisfy the needs of the medical sector for self-powered miniaturized point-of-care devices (SPOCD), multifunctional advanced materials are increasingly employed for the fabrication and development of electrochemical sensors and energy devices. Beyond healthcare diagnostics, such sensors are also needed for food quality analysis, environmental monitoring,

pharmaceutical analysis, and monitoring of industrial bioproduction processes. For the development of SPOCDs, the three significant functional elements of a successful biomedical sensor are flexible substrate, power supply, and capacity for specific and sensitive detection of biomolecules. Thus, the integration of fuel cells and electrochemical sensors with a flexible substrate can meet all the needs for wearable, flexible, and miniaturized SPOCDs.

Various polymers have been proposed as the flexible substrates for SPOCDs, such as polyimide (PI), polyethylene terephthalate (PET), polycarbonate (PC), polyvinyl alcohol (PVA), polyethylene naphthalate (PEN)), etc. Among these, PI stands out by its low cost and availability. Facility of surface modification is an important feature of flexible polymer substrates. Various fabrication methods employed to modify

and develop conductive flexible electrodes, such as e.g., photolithography, involve complex multistep surface modification procedures. Facile surface modification, using versatile metal nanoparticles (MNPs) can be a viable alternative. Thermal evaporation/sputter deposition of MNPs on the flexible polymer surface allows for a combination of flexibility with an efficient electron transfer rate and ultra-sensitivity [1–14].

In view of their physicochemical and electrochemical properties, several metals are used as electrocatalysts: Ag, Au, Co, Cu, Mn, Ni, Pt, Pd, etc. Among these, Pd gained significant attention due to its abundance, good electrocatalytic effect, and large accessible electroactive surface area. Also, Pd exhibits outstanding electrocatalytic properties in the alkaline medium, reacting with small biomolecules (alcohols, sugars), making it suitable for sensors and fuel cell devices [14–21]. In addition to metals, conducting polymers (CPs) also holds a important role in the fabrication of wearable, flexible, and multifunctional electrochemical devices. Among various CPs, polyaniline (PAN) stands out due to its easily tunable electrical conductivity, simple processability, stability, low cost, reversible redox properties, and continuous matrix with strong adhesion. Furthermore, combinations of CPs and MNPs in nanocomposites were found to display outstanding properties in sensor and energy devices, due to their synergetic interaction. Among such CP-MNP composites, a combination of PAN and Pd NPs gives rise to strong and stable adherence with the electrode, accompanied by outstanding electrochemical oxidation, uniform dispersion, and many electroactive spots which ensure fast ionic diffusion [22–28].

Glucose is a common target analyte for medical biosensors, due to the need for monitoring blood glucose levels in diabetic and pre-diabetic patients. Ultra-sensitive and highly selective sensors for glucose are not only applicable for monitoring blood sugar, but are also employed in e.g., bioprocessing, the food industry, and the development of renewable, sustainable fuel cells. Many different approaches are currently being developed for glucose sensing, including enzyme-based and receptor-based electrochemical biosensors. Although these sensors yield good output, their use is restricted due to unavoidable difficulties such as deactivation, instability, and enzyme denaturation [29–32]. On the other hand, to make the device easily operable outside the laboratory the solution will be the integration of multifunctional electrochemical energy devices together. To acquire SPOCD analytical platforms, several illustrations of these kinds of schemes have been reported in the literature, with methanol-KOH fuel cells, hydrogen fuel cells, formic acid fuel cells, and ethanol-dichromate fuel-oxidant mixture [33–38]. All of these electrochemical systems seem to be proficient in driving small multifunctional devices.

Still, there is a significant challenge among electrochemical researchers that the selection of a suitable multifunctional electroactive material and its synthesis and fabrication as an outstanding electrocatalyst (ect) with superior electrocatalytic properties remains an obstacle. To overcome these issues, here in our work we fabricated a flexible (PI/Au substrate), multifunctional electroactive nanocomposite electrode based on PI/Au-PAN/Pd by the one-step electrochemical deposition technique (overall scheme Fig. 1). The physicochemical and electrochemical characterization authenticates the successful synthesis toward a non-enzymatic glucose sensor and efficient direct alcohol fuel cell application (DAFCs) (methanol and ethanol oxidation reaction).

2. Experimental process

2.1. Materials used

Aniline, potassium hydroxide, sodium hydroxide, palladium chloride, sulfuric acid, methanol, $D^{(+)}$-glucose, sodium chloride, ascorbic acid, lactose, dopamine, artificial saliva, acetone, and ethanol were obtained from Sigma-Aldrich (USA). All the chemicals engaged in the investigational procedure were of research grade and engaged as arrived without any purification. Polyimide (PI) substrates of 125 μm thickness
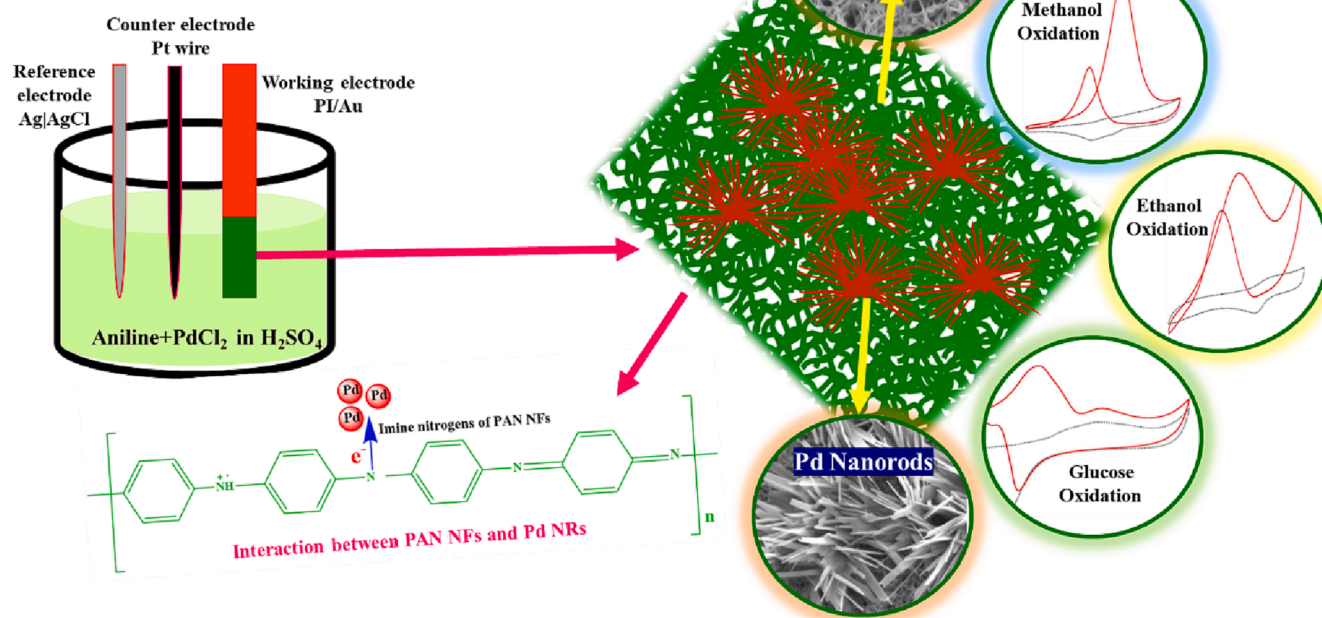

Fig. 1. Overall scheme from electrochemical deposition to applications.

were used to fabricate the electrodes purchased from Corix3D, Sweden.

2.2. Fabrication of PI/Au flexible electrodes

To fabricate the PI/Au-PAN/Pd (PI substrate of 1 cm^2 was engaged), the polymer substrate was sonicated for 15 min in acetone to get rid of the debris and dust particles from the surface of the flexible electrode. After cleaning, the flexible polymer electrode was cleaned with ethanol and DI water and dried up completely with N$_2$ gas. A coating of Cr/Au (5/100 nm) was homogeneously deposited on the cleaned PI electrode surface with a thermal evaporation technique.

2.3. Electrochemical deposition of PAN/Pd on the PI/Au flexible electrodes

PI/Au-PAN/Pd nanocomposite was prepared electrochemically according to our previously reported process with small changes [28]. In detail, aniline (60 mM) and PdCl$_2$ (0.01 M) were dissolved in 0.5 M H$_2$SO$_4$, which turns into a cloudy-colored solution. The mixture was then stirred for 15 min to attain a homogenous mixture until it gets a transparent light-yellow color. Then, the prepared PI/Au flexible electrode was immersed in the electrochemical cell containing the homogenous mixture as a working electrode. Next, the cyclic voltammetry (CV) was executed in the potential width from − 0.2 to 1 V at a scan rate of 100 mV/s for 20 continuous cycles (Fig. S1). During the electrochemical deposition, the PAN/Pd (dark green) nanocomposites were grown over the PI/Au electrode surface, and the fabricated flexible electrode was gently rinsed with DI water and dried out at ambient temperature. The deposited electroactive mass was weighed to be 10 mg and engaged as a modified electrode towards electrooxidation. For comparison, PI/Au-PAN electrodes were also fabricated under the same experimental steps. When not in use, the fabricated flexible electrodes were stored in dry conditions.

2.4. Instrumentations used

X-ray diffraction (XRD) structural patterns were documented in the range of 10–80° on a Bruker D8 Discover diffractometer by CuKα radiation (λ = 1.542 Å 40 mA, 40 kV). The surface morphological views of the electrodeposited nanocomposite-modified flexible electrodes were visualized using a field-emission scanning electron microscope (FESEM - JEOL 7800F Prime). Fourier-transform infrared (FTIR) molecular vibrations were recorded using the FTIR microscope/spectrometer-Bruker Hyperion3000/Vertex70v. The electrochemical analysis such as CV, electrochemical impedance spectroscopy (EIS), and differential pulse voltammetry (DPV) was studied with a computerized electrochemical workstation- CHI6048E, 220 V AC, 0.4A (CH Instruments Inc., Texas, USA). A conventional 3-electrode setup with Ag/AgCl (3 M KCl saturated)-reference electrode, Pt wire-counter electrode, and PI/Au-PAN/Pd, PI/Au-PAN, and PI/Au flexible electrodes were employed as working electrodes. Elemental analysis was done by using PHI5000 Versa Probe III X-ray photoelectron spectroscopy (XPS) instrument.

2.5. Procedure for electrochemical oxidation of glucose (EOG)

The experimental parameters for EOG CV measurement were as follows: sampling interval of 1 mV/s, scan rate of 100 mV/s, quiet time of 2 s, and a sensitivity of 10^{-3} (A/V) with an applied potential width from −0.2 V to 0.8 V. DPV analysis were carried out in the same potential width. 0.1 M NaOH is engaged as an electrolyte background for glucose electrooxidation.

2.6. Procedure for electrocatalytic methanol and ethanol oxidation reaction (EOM and EOE)

The EOM and EOE of the flexible nanocomposite electrode were studied in 0.5 M KOH solution containing 1 M methanol and ethanol by CV in the applied potential width from −0.6 to 0.2 V at a scan rate of 100 mV/s. The stability and molar concentration of the modified flexible electrodes were also measured in the same environment.

3. Results and discussion

The fabricated multifunctional electrode's structural geometry, functional group analysis, and morphological views were investigated using XRD, FTIR, and FESEM. All the results coincide with each other and reveal successful electrodeposition over the flexible PI/Au electrode. The authenticated flexible electrodes with rapid electron transfer, high electrical conductivity, and high ionic diffusion with more electroactive spots lead to excellent electrochemical oxidation of glucose, methanol, and ethanol as follows (as depicted in Fig. 1).

3.1. Semicrystalline structural geometry of PAN/Pd using XRD

After the deposition of PAN nanofibers (NFs) and Pd nanorods (NRs) on the flexible PI/Au substrate, the surface was characterized by XRD (Fig. 2A). Fig. 2(a) revealed that the electrodeposited PAN was semi-crystalline and displays peaks at 2θ = 26.2° corresponding to the miller indices (200). This semi-crystallinity is due to the quinoid and benzenoid ring repetition in the continuous structural organization of the PAN NF chain. In addition to the PAN NFs peak (26.2°), new diffraction peaks were observed at 2θ = 38.5°, 54°, and 77.7° in the pattern of PAN/Pd [39–41], which indicates the presence and continued existence of a semi-crystalline PAN along with the highly crystalline Pd NRs diffraction peaks (JCPDS 05–0681) [42]. These compared results confirm the successful electrodeposition of the multifunctional PAN/Pd electrocatalyst on the flexible PI/Au substrate.

3.2. Molecular vibration analysis confirms the redox interaction of PAN NFs and Pd NRs

The molecular vibrational investigations describe the characteristic functional group signatures of the fabricated electrocatalyst materials in Fig. 2B. The PAN structure ensures the benzenoid and quinoid forms of the aromatic phenyl ring structure by two distinct characteristic signatures at 1502 and 1618 cm^{-1}, respectively. The C-N and C $=$ C stretching of benzenoid rings show peaks around 1238, and 1475 cm^{-1}, and C-N and C $=$ C stretching of quinoid structures show peaks at 1338, and 1581 cm^{-1}, correspondingly. Due to the interaction with Pd NRs, the signatures of PAN NFs have a minor shift in signatures from the benzenoid and quinoid structure at higher wavelengths of patterns (Fig. 2B (inset). Also, as shown in Fig. 2B (inset), a slightly higher relative intensity quinoid and benzenoid (Iq/Ib) of C $=$ C stretching vibrations was observed that could be the evidence for the redox reaction between PAN NFs and Pd NRs [28,39]. These distinctive IR signs authenticate the functional groups of PAN NFs and their synergistic interaction with Pd NRs which are highly accountable for the electrooxidation of glucose and alcohols.

3.3. Morphological and elemental investigations

Fig. 3 depicts the morphological investigations through FESEM (A) PAN NFs, (B) higher magnification of PAN nanofibers, (C) PAN NFs with Pd NRs (nanorods), and (D) EDX: the composition of flexible electrodes. The PAN NF acquired morphology from 20 consecutive electrodeposition cycles appears to be a long cross-linked, thin, and smooth NFs network structure. The size of PAN NFs ranges from 80 to 100 nm which are smooth and continuous without agglomeration as shown in the magnified version (Fig. 3B). These NFs act as an excellent substrate matrix and facilitate the large accessible surface area for depositing the electrochemically active Pd NPs. Further, Pd nanorods (NRs) were captured over the PAN NFs as shown in Fig. 3C. The captured Pd NRs
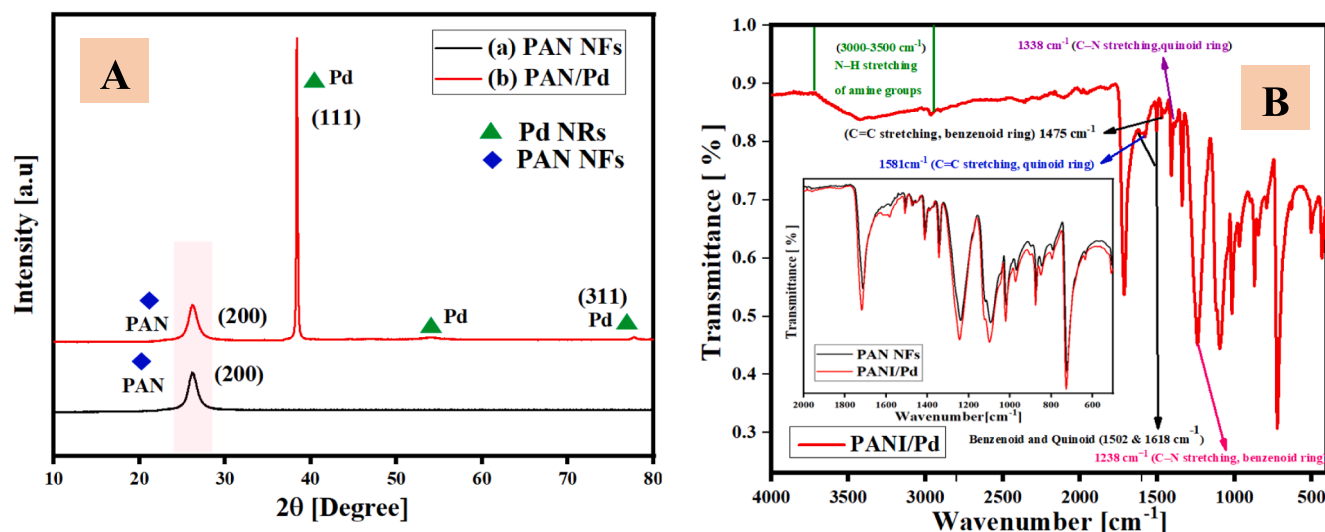
Fig. 2. (A) Structural geometry of (a) PAN NFs and (b) PAN/Pd flexible electrodes and (B) molecular vibrational analysis of PAN/Pd flexible electrocatalyst (inset: comparison of PAN NFs (black line) and PAN/Pd (red line)). (For interpretation of the references to color in this figure legend, the reader is referred to the web version of this article.)

have a diameter ranging from 80 to 150 nm and a length of a few micrometers. These NFs and NRs morphological structures belong to the combination of Carbon (C), Nitrogen(N), Oxygen (O), and Palladium (Pd) elements that were confirmed by EDX and mapping analysis as depicted in Fig. 3D and Fig. S2.

Fig. 3(E-I) depicts the survey spectrum investigations and the characteristic spectrum for carbon, nitrogen, oxygen, and Pd that ensure the successful fabrication of PAN/Pd multifunctional electrocatalyst. Fig. 3F shows the C1s pattern of PAN/Pd flexible electrode with two binding energy (BE) waves at 284.6 and 287.2 eV which can be corresponds to primary carbon and the carbon connection with oxygen or nitrogen. The N1 core spectrum of Fig. 3G validates the existence of a major peak at 399.3 eV ascribed to the –NH- amine group of PAN. The spectral characteristics of Pd 3d is shown in Fig. 3H. The Pd peaks contain two splitting doublets for the PAN/Pd electrocatalyst, and the dual BE peaks at ~ 336 and ~ 340.8 eV are ascribed to the existence of metallic Pd. It is observed that the PAN/Pd electrocatalyst displays an improved substance of the metallic Pd elements, and it is anticipated to the amine group's occurrence in the carbon support may fairly resist the re-oxidation of metallic Pd resources in environmental conditions, resulting in an augmented Pd^0 level. Because of amine grouping in the combination of PAN/Pd electrocatalyst, probably facilitates electrochemical immobilization of the metallic Pd^0 and also inhibits the oxidation of metallic Pd [28]. Also, the recorded spectra at higher BE are attributed to the oxidized carbon (C-O) elements as shown in Fig. 3I.

These ensured morphological and elemental nanostructure analyses made of PAN NF chains with Pd NRs provide abundant electrochemically active spots which promote high ionic diffusion to achieve excellent electrooxidation.

3.4. Electrochemical analysis

3.4.1. Cyclic voltammetry and electrochemical impedance spectroscopy (EIS) investigations

The electrochemical signature of the PAN nanofibers and single-step co-deposited PAN-Pd on PI/Au flexible substrate were recorded in the potential width −0.2 to 1.0 V at a scan rate of 100 mV/s in H$_2$SO$_4$ as the background electrolyte. CV patterns of PAN NFs (Fig. S1) depicted four pairs of redox (oxidation/reduction) waves, oxidation signatures around 0.30, 0.50, 0.60, and 0.92 V with respective cathodic counterparts around 0.02, 0.38, 0.45, and 0.75 V, correspondingly. The redox signature around 0.30/0.20 V ascribes to the formation of the radical

cation, and the second wave at 0.50/0.38 V represents the development of benzoquinone. The third and fourth redox waves at 0.60/0.45 V and 0.92/0.75 V describe the oxidation of head-to-tail dimer and emeraldine to pernigraniline structure conversion, correspondingly. On the other hand, the recorded redox peak of Fig. 4A(c) depicts the highest peak current density in comparison with the PAN NFs and PI/Au substrate (Fig. 4A(a&b)). This performance is ascribed to the larger number of accessible electroactive surface spots existing for adsorption on the material's surface and facilitates an excellent storage material [28]. All these electrochemical signatures of PAN NFs and Pd NRs ensure the successful electrodeposition of PAN/Pd on PI/Au flexible electrodes. In addition, the Randles–Sevcik equation is used to understand the electrochemical performance by calculating the electrochemically active surface area for the fabricated multifunctional electrocatalyst nanostructures (equation (1)) [30].

$$Ip = 2.69*10^5*A*C*n^{2/3}*D^{1/2}*V^{1/2} \rightarrow \quad (1)$$

Here Ip is the redox peak current, A is the area of the electrochemically active surface area in cm^2, C is the bulk concentration of the redox species used, n is the number of electrons transported per redox event, where n = 1, D is the diffusion coefficient is 6.70×10^{-6} cm^2/s, and V- is the scan rate potential (in our case 100 mV/s). Based on equation (1), the electrochemical surface area for the bare PI/Au, PI/Au-PAN NFs, and PI/Au-PAN/Pd nanocomposite structures was calculated as 0.039, 0.117, and 0.214 cm^2, respectively. The boosted-up electrochemically active surface area of the PAN NFs with Pd NRs confirms the synergy effect of the Pd NRs (as shown in Fig. 4C) to offer an efficient platform and large accessible surface in simplifying electron passage between the target solution and the modified multifunctional electrode.

Next, EIS analysis helped in the evaluation of performance and interfacial properties of bare and electrodeposited flexible electrodes in 5 mM Fe (CN)$_6^{3-/4-}$ comprising 0.1 M KCl as the electrolyte background (Fig. 4B). Also, an equivalent circuit was made to fit the EIS data points as depicted in Fig. 4B (inset). The equivalent circuit consists of solution resistance (R$_s$), constant phase element (CPE), charge transfer resistance (R$_{ct}$), and Warburg impedance (frequency-dependent variable), respectively. As shown in the figure, at high-frequency regions, lower R$_{ct}$ was observed which leads to rapid electron transfer. The surface diffusion process of the fabricated materials was ensured by the linear line after a small deflection i.e., from the Rct value. This highlights the improved electrical conductivity of the modified multifunctional flexible electrode which coincides with the CV analysis. The R$_{ct}$ of the PAN/Pd (207 Ω)
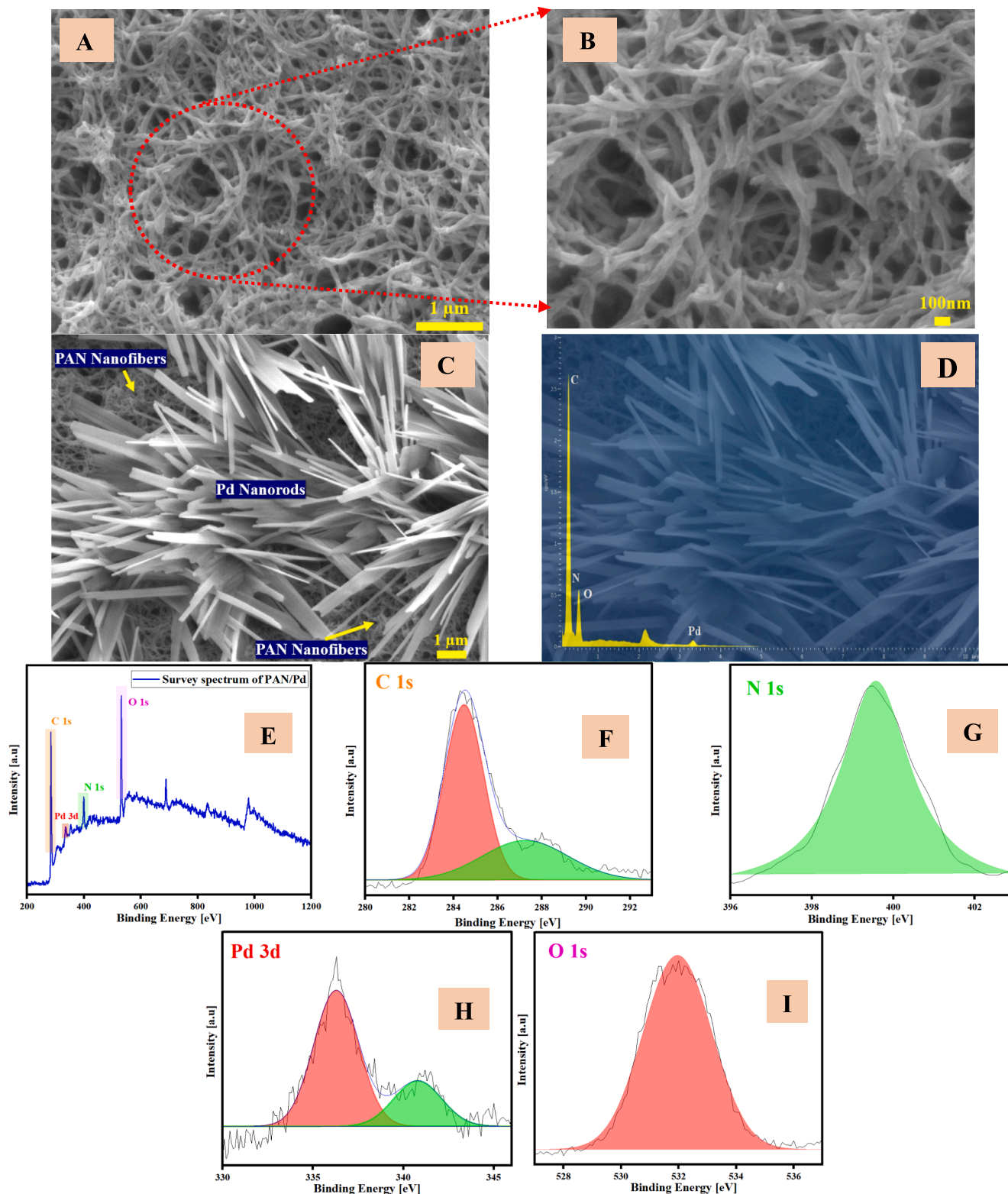
Fig. 3. Morphological investigations: (A) PAN nanofibers, (B) higher magnification of PAN nanofibers, (C) PAN NFs with Pd nanorods, and (D) EDX: composition of flexible electrodes. Elemental analysis: (E) XPS survey spectrum of PAN/Pd (F) C1s, (G) N1s, (H) Pd 3d, and (I) O1s XPS spectra.

(Fig. 4B (inset)) is lower than the PAN nanofibers (1052 Ω) which help in an efficient electrooxidation pathway with high ionic diffusion. From the CV and EIS analysis, it is noticed that the PAN/Pd flexible electrodes (dark green) possess a superior accessible active surface area and high electrical conductivity. By considering the effective electrochemical properties, PAN/Pd flexible electrodes were engaged in all the experiments towards glucose, methanol, and ethanol electrooxidation.

3.4.2. EOG reaction investigations

3.4.2.1. EOG mechanism of reaction and comparison studies. Fig. 5A depicts the CV patterns of PI/Au-PAN/Pd flexible electrodes with and
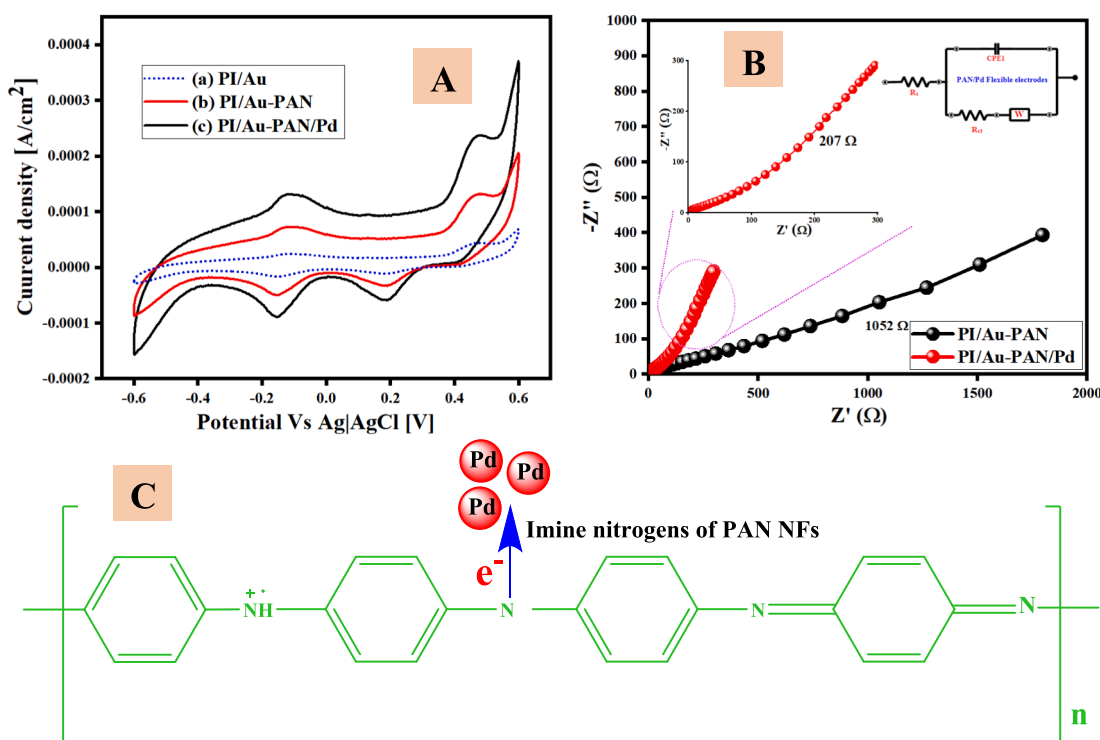
Fig. 4. (A) (a) PI/Au, (b) PI/Au-PAN NF, and (c) PI/Au-PAN/Pd in 0.5 M H$_2$SO$_4$ at a sweep rate of 100 mV s^{-1}. (B) EIS spectra of PI/Au-PAN, and PI/Au-PAN/Pd flexible electrodes recorded in 0.1 M KCl containing 2 mM [Fe(CN)$_6$]$^{3-/4-}$. Insets: Magnified portion and equivalent circuit of PI/Au-PAN/Pd electrode. (C) Mechanism of interaction between PAN NFs and Pd NRs.

without the addition of 50 μM glucose in a 0.1 M NaOH electrolyte background. The electrically conductive PI/Au-PAN/Pd flexible electrode in 0.1 M NaOH background displays (Fig. 5A**(a)** without the addition of glucose) the characteristic palladium peaks counting the palladium oxide (PdO) formation, the reduction of PdO, and the hydrogen adsorption/desorption (H$_{ad}$/H$_{des}$) region. This reveals that there are more electroactive spots present on the electrode surface. Compared to the solution without glucose, a significant increase in the oxidation current value with applied potential was clearly detected after glucose addition as shown in Fig. 5A**(b)**. Upon the glucose injection, an anodic peak at 0.16 V is detected in the positive potential scan of the PI/Au-PAN/Pd flexible electrode, which is ascribed to indirect glucose oxidation. For example, the electro-adsorption of 1 molecule of glucose roots the adsorbed intermediate generation, and one glucose molecule drops one proton in this electrooxidation process [42]. It could be ensured by the sum of the indirect glucose oxidation peak current area and the reduction peak current area of Pd (OH) equivalent to the oxidation peak current area of Pd NRs. This outcome validates that the PI/Au-PAN/Pd flexible electrode is a perfect applicant for glucose detection quantitatively.

Equation (2) and (3) represents the possible EOGR at the PI/Au-PAN/Pd flexible electrode in an alkaline medium at 0.1 M NaOH during the electrochemical oxidation process [29,42].

$$Pd \ + \ OH^- \rightarrow PdOH \ + \ e^- \rightarrow \qquad (2)$$

$$PdOH + glucose \rightarrow Pd + gluconolactone \rightarrow \qquad (3)$$
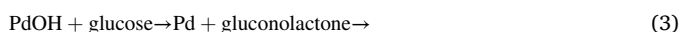
The above EOGR is well reliable with the CV results of the PI/Au-PAN/Pd flexible electrode with and without the addition of glucose (Fig. 5A**(a,b)**). In the CV curve of the multifunctional electrode without glucose, at first, the metal Pd NRs is oxidized to Pd(OH) during the positive scan, and in the negative scan, the obtained Pd(OH) is totally reduced to Pd again, which can be substantiated by the same area of redox peaks. But in the case of PI/Au-PAN/Pd flexible electrode, with

the addition of glucose, the part of the formed Pd (OH) is used up for the electrooxidation of glucose into gluconolactone in the positive potential scan, and during the negative potential scan, the remaining Pd (OH) part is reduced to Pd again [40].

Thus, the mechanism of electrooxidation using a metal (Pd NRs here) undergo the following steps, First, the metal starts to oxidize at a lower potential on the electroactive electrode surface. Next, the oxidized metal ion acts as an electro-oxidant and helps in the conversion of glucose to gluconolactone and hydrolyzed to gluconic acid in the background solution.

3.4.2.2. Electrochemical glucose sensing characteristics. Fig. 5B **(a-j)** depicts the CV patterns of the PI/Au-PAN/Pd flexible electrode with the addition of different molar concentrations of glucose (10 to 100 μM) in a 0.1 M NaOH electrolyte background. The acquired results indicate the linear response of CV patterns in the potential width from −0.1 to 0.8 V as illustrated. Upon each addition of glucose concentration, the indirect glucose oxidation peak current rises with the injection of glucose concentration from 10 to 100 μM. This is due to the amount of oxidized and adsorbed glucose molecules on the electrode's surface which increases as the concentration of glucose rises. The glucose concentration ranging from 10 to 100 μM exhibited a linear calibration plot (Fig. 5C) with a regression coefficient of R^2 = 0.984, sensitivity (slope of the calibration plot/active surface area) as 2140 μA/μMcm^2, the limit of detection (LOD) of 0.3 μM and rapid response (~2 s).

Also, the performance analysis of the flexible multifunctional electrode has been compared with other reported literature and tabulated in Table S1. The comparison analysis illustrates that the fabricated flexible electrode exhibits rapid response and a low detection limit with ultra-high sensitivity.

3.4.2.3. Differential pulse voltammetry, interference, and real sample analysis. Differential pulse voltammetry (DPV) is a highly sensitive and efficient tool to quantify glucose concentration, hence, the DPV was
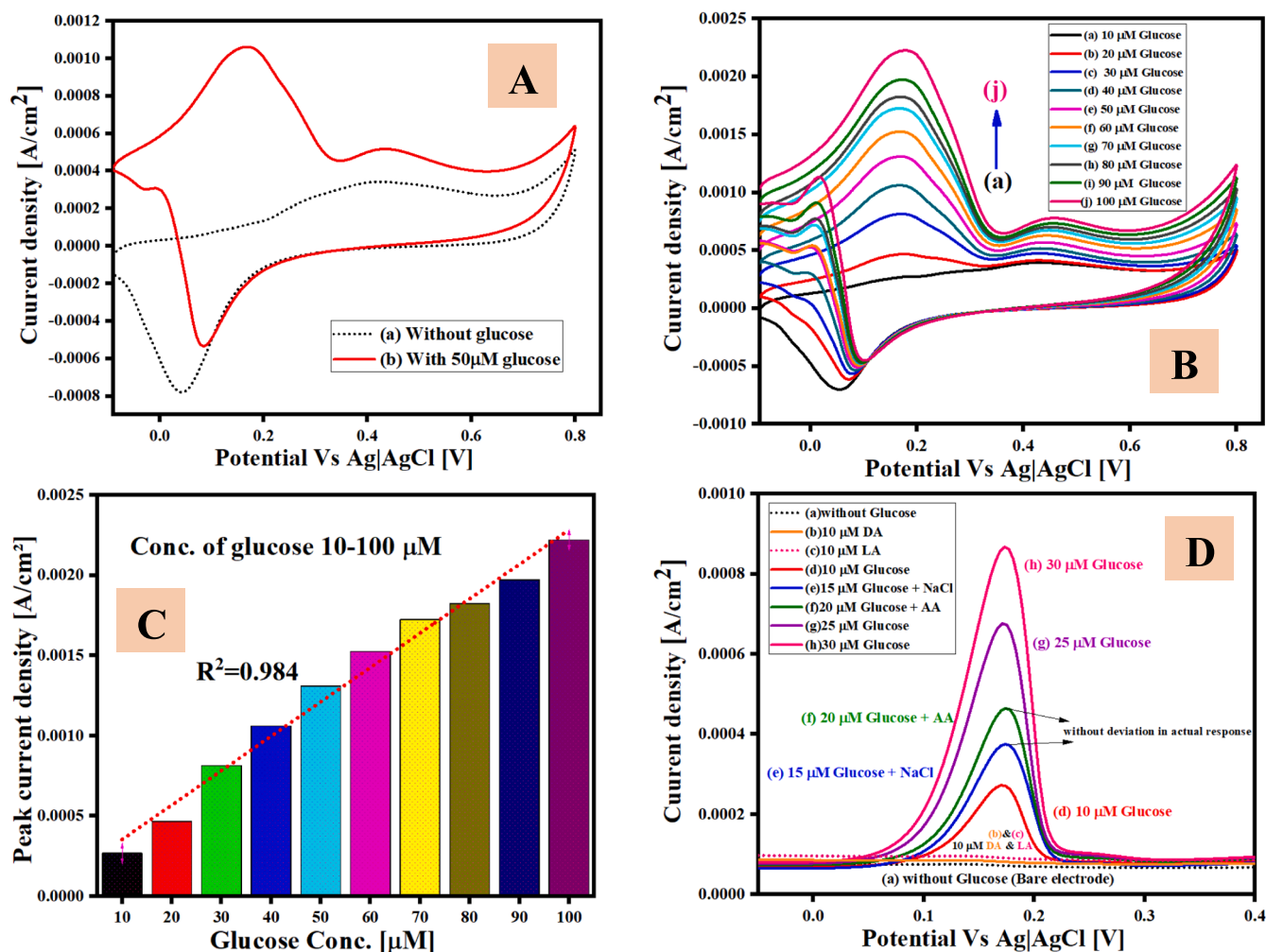
Fig. 5. (A) CV obtained in 0.1 M NaOH at a scan rate of 100 mV/s of PI/Au-PAN/Pd flexible electrodes at (a) without, and (b) with glucose, (B) CV peaks of different concentrations from 10 to 100 μM of glucose, (C) Linear calibration plot of various molar concentrations of glucose, and (D) DPV analysis of (a) without and (b) with the addition of 10 μM DA, (c) 10 μM LA, (d) 10 μM glucose, (e) 15 μM glucose + NaCl, (f) 20 μM + AA (g) 25 μM glucose, and (h) 30 μM glucose.

employed for glucose detection. Fig. 5D **(a-h)** displays the DPV responses of glucose electrooxidation curves for PI/Au-PAN/Pd flexible electrode in 0.1 M NaOH electrolyte solution containing various concentrations of glucose ranging from 10 to 30 μM along with the interfering species. As depicted, in comparison with bare electrolyte background (i.e., without the addition of glucose) a sharp oxidation response peak appeared for every addition of glucose, the oxidation peak current density was also sequentially amplified with increasing concentrations.

Further, interference analysis is an important parameter to be considered in real-time applications. Thus, the coexisting species such as dopamine (DA), lactose (LA), sodium chloride (NaCl), and ascorbic acid (AA) which have the same oxidational potential as glucose were investigated using DPV. As shown in Fig. 5D, the addition of 10 μM (DA, LA, NaCl, AA) did not alter the peak current response. Thus, an insignificant perturbation peak current after the addition of electro-active interfering species reveals that fabricated multifunctional electrode is highly selective towards glucose.

The normal glucose concentration range in the saliva is 20–240 μM [30]. The electrochemically modified PI/Au-PAN/Pd flexible electrode is appropriate for its real-world application in non-invasive glucose detection in saliva. To examine its practicality and selectivity, the multifunctional modified flexible electrode was employed for the determination of glucose in modified artificial saliva (AS) using the standard addition technique. The precision of the fabricated electrode

was estimated by a recovery test. Three different samples/amounts of glucose were spiked in AS and the retrieval outcomes were tabulated in Table S2. The modified electrode demonstrated good recovery of ∼ 96.6–98.2 % validating its practical applications.

3.4.2.4. Stability, Reproducibility, and practicability analysis of the flexible electrode. To further evaluate the potential for practical usage, the fabricated PI/Au-PAN/Pd multifunctional flexible electrode's stability and reproducibility were also evaluated. The CV of the flexible electrode in 0.1 M NaOH with 10 μM glucose at a scan rate of 100 mV/s was tested for 200 consecutive cycles. The peak current density of the 1st, 50th, 100th, 150th, and 200th cycles was taken and compared to illustrate the stability of the modified electrode. As depicted in Fig. 6A, after 200 consecutive potential cycles, the peak current density sustains 98.46% of the original value. The cycle life of the modified electrode was also examined by investigating its peak current density in the presence of 10 μM glucose during storage at a 4 °C room for 30 days. Fig. 6B depicts that the flexible electrode could steadily maintain its initial sensitivity up to 95.65% after 30 days. These outcomes corroborate the excellent stability of the modified electrode. Further to ensure reproducibility, the peak current density responses of 4 identically modified electrodes were tested towards 10 μM glucose. As shown in Fig. 6C, the modified electrodes demonstrate a relative standard deviation (RSD) of around ∼ 1.4%, signifying the high reproducibility of the sensor.
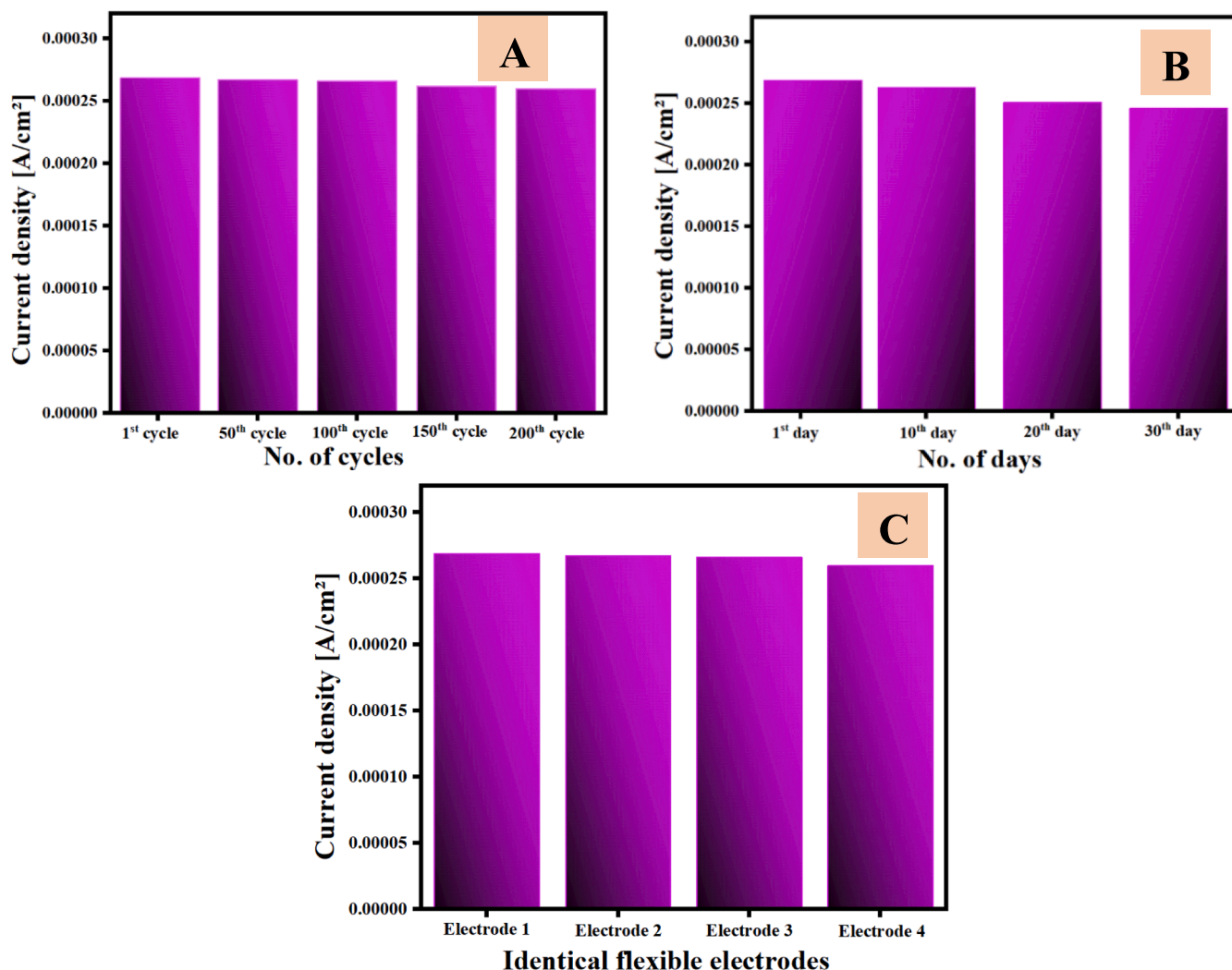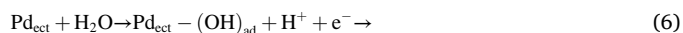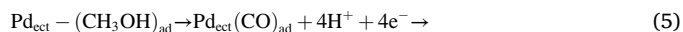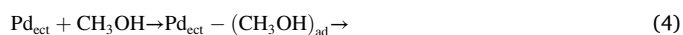
Fig. 6. Stability analysis of the modified flexible electrode with respect to (A) number of cycles, (B) number of days, and (C) Identical flexible electrodes.

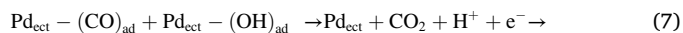*3.4.3. Electrocatalytic investigations towards direct alcohol fuel cell (DAFC) applications*

3.4.3.1. EOM reaction and stability of the flexible electrode. To examine the methanol electrooxidation performance of the PI/Au-PAN/Pd flexible electrode, 0.5 M KOH was used as a background electrolyte solution. Fig. 7A shows the cyclic voltammetric pattern of PI/Au-PAN/Pd with and without 1 M methanol. In Fig. 7A(a), the bare KOH pattern depicts both the absorption and adsorption of hydrogen on the Pd surface, also it exhibits the formation and reduction of PdO as well as the formation of benzoquinone facilitating more electroactive sites for both the methanol and ethanol electro-oxidation. A well-noticed CV pattern acquired at forward and reverse potential scans of EOM give rise to two oxidation peaks. The first CV peak is at -0.09 V with a current density of 3 mA/cm^2 (forward potential scan) and the next is at -0.27 V with a current density of 1 mA/cm^2 (reverse potential scan) as shown in Fig. 7A(b). Typically, in ECMO reaction at the forward potential scan (I_{fp}), the peak current density indicates the dehydrogenation of methanol adsorbed to yield Pd-adsorbed carbonaceous elements like CO. While the peak current density at the reverse potential scan (I_{rp}) generally designates the electrochemical oxidation of adsorbed carbonaceous types like CO.

The well-recognized ECMO reaction mechanism follows the formate ions production alike the acetate ions (equations (4–7)) [22,28].

In forward potential scan

$$Pd_{ect} + CH_3OH \rightarrow Pd_{ect} - (CH_3OH)_{ad} \rightarrow \tag{4}$$

$$Pd_{ect} - (CH_3OH)_{ad} \rightarrow Pd_{ect}(CO)_{ad} + 4H^+ + 4e^- \rightarrow \tag{5}$$

$$Pd_{ect} + H_2O \rightarrow Pd_{ect} - (OH)_{ad} + H^+ + e^- \rightarrow \tag{6}$$

In reverse potential scan

$$Pd_{ect} - (CO)_{ad} + Pd_{ect} - (OH)_{ad} \rightarrow Pd_{ect} + CO_2 + H^+ + e^- \rightarrow \tag{7}$$

Additionally, different concentration ranging from 1 to 10 M methanol was injected successively and the CV pattern was noted (Fig. 7B). The maximum peak current density reaches 6.5 mA/cm^2 at -0.09 V (10 M of methanol) while at the reverse scanning, the maximum current grows to 2.6 mA/cm^2 at 10 M from 1 mA/cm^2 at 1 M at -0.27 V. The CV patterns depict the linear rise and no downslope in the electrooxidation of methanol when injecting various concentration ratios from 1 to 10 M. Hence, the substantial enhancement attained by PI/Au-PAN/Pd flexible electrode towards the EOM. Fig. 7C designates the redox current density of methanol linearly augmented with the rising square root of the sweep rate (Regression coefficient R^2 = 0.995 and 0.992). This signifies that EOM at PI/Au-PAN/Pd flexible electrode follows via a diffusion-controlled progression [22,28] at the electrochemically deposited, tailored flexible electrolyte/electrode interface.

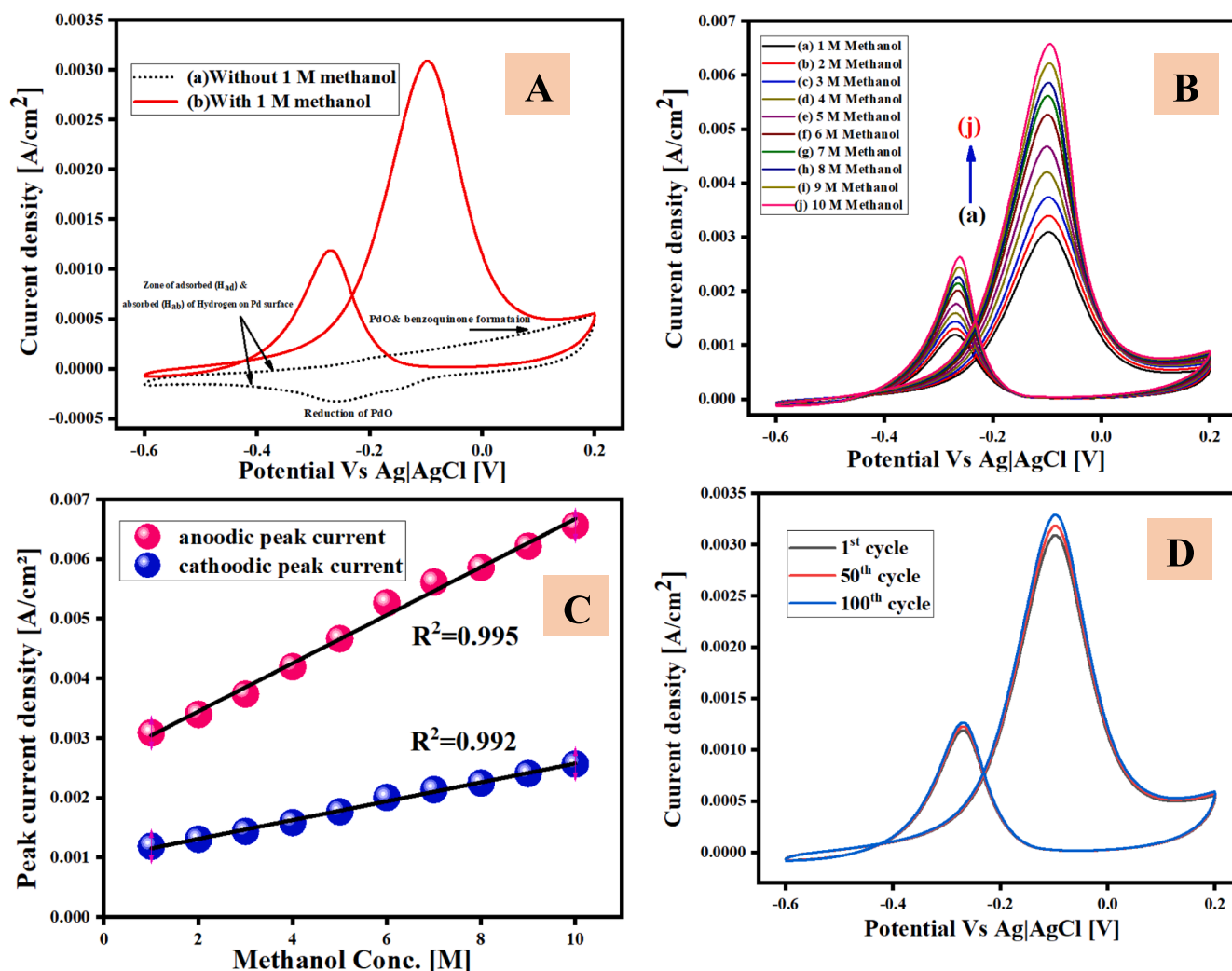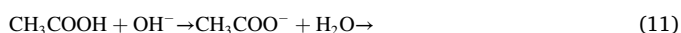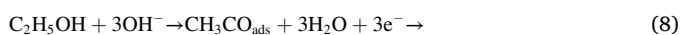*3.4.3.2. EOE reaction and stability of the flexible electrode.* The same

Fig. 7. CV of PI/Au-PAN/Pd flexible electrodes (A) (a) absence and (b) presence of 1 M Methanol at a sweep rate of 100 mV s^{-1}, (B) CV peaks of different concentrations from 1 to 10 M of methanol, (C) anodic and cathodic peaks of various molar concentrations, and (D) stability analysis for 1 M methanol at 1st and 100th cycles. All at an electrolyte background of 1 M KOH solution.

electrolyte background and the potential width ranging from −0.6 to 0.1 V have been employed for the electro-oxidation of ethanol. Fig. 8A shows the cyclic voltammetric pattern of PI/Au-PAN/Pd (a) without and (b) with 1 M ethanol. Fig. 8A(**b**) depicts the CV pattern for the EOE reaction of 1 M in an alkaline background electrolyte and there is a clear electrooxidation of ethanol in comparison with bare KOH. The well-noticed CV patterns acquired at forward and reverse potential scans of EOE ended with two oxidation peaks. The first CV peak is at − 0.24 V with a peak current density of 0.96 mA/cm^2 (forward potential scan) and the next is at − 0.32 V with a peak current density of 0.67 mA/cm^2 (reverse potential scan). The renowned electro-oxidation reaction mechanism of ethanol [22] is as follows (equations 8–11),

$$C_2H_5OH + 3OH^- \rightarrow CH_3CO_{ads} + 3H_2O + 3e^- \rightarrow \qquad (8)$$

$$OH^- \rightarrow OH_{ads} + 1e^- \rightarrow \qquad (9)$$

$$CH_3CO_{ads} + OH_{ads} \rightarrow CH_3COOH \rightarrow \qquad (10)$$

$$CH_3COOH + OH^- \rightarrow CH_3COO^- + H_2O \rightarrow \qquad (11)$$

The molar concentration of the ethanol oxidation reaction is depicted in Fig. 8B from 1 to 10 M ethanol. The maximum current peak rise is 3 mA/cm^2 and in reverse potential scanning, the maximum current peak reaches over 3 mA/cm^2 from 0.96 mA/cm^2 and 0.67 mA/cm^2 for 10 M

ethanol concentration. There is a minor variation that arises during the ethanol addition to varying the concentration from 1 to 10 M, that is owing to the diffusion layer establishment, and it grounds the high electrical conductivity. Fig. 8C defines the redox current density of ethanol linearly augmented with the rising square root of the sweep rate (R^2 = 0.987 and 0.993), which represents the ethanol oxidation at a modified flexible electrode followed over a diffusion-controlled development at the electrolyte/electrode interface.

3.4.3.3. Stability analysis of the flexible electrode for EOM and EOE reactions. The linear stability performance of the electroactive anode PI/Au-PAN/Pd flexible electrode material was investigated using the CV technique and illustrated in Fig. 7D and 8D. Here, the 1st cycle and 100th cycle of EOM and EOE at 1 M concentration are depicted. In the data, we observed a small rise in the peak current with a rise in the number of cycles without any declination, which might be due to the partial dissolution loss of the electrocatalyst and the hazardous intermediate accumulation arising in the electrochemical oxidation progression [22,28]. Therefore, it demonstrates the outstanding stability of flexible, multifunctional nanocomposite electrodes even after the 100th cycle.

Also, the performance analysis of the flexible multifunctional electrode has been compared with other reported literature in terms of its electronegativity, and the methodology was tabulated in **Table S3**. Due
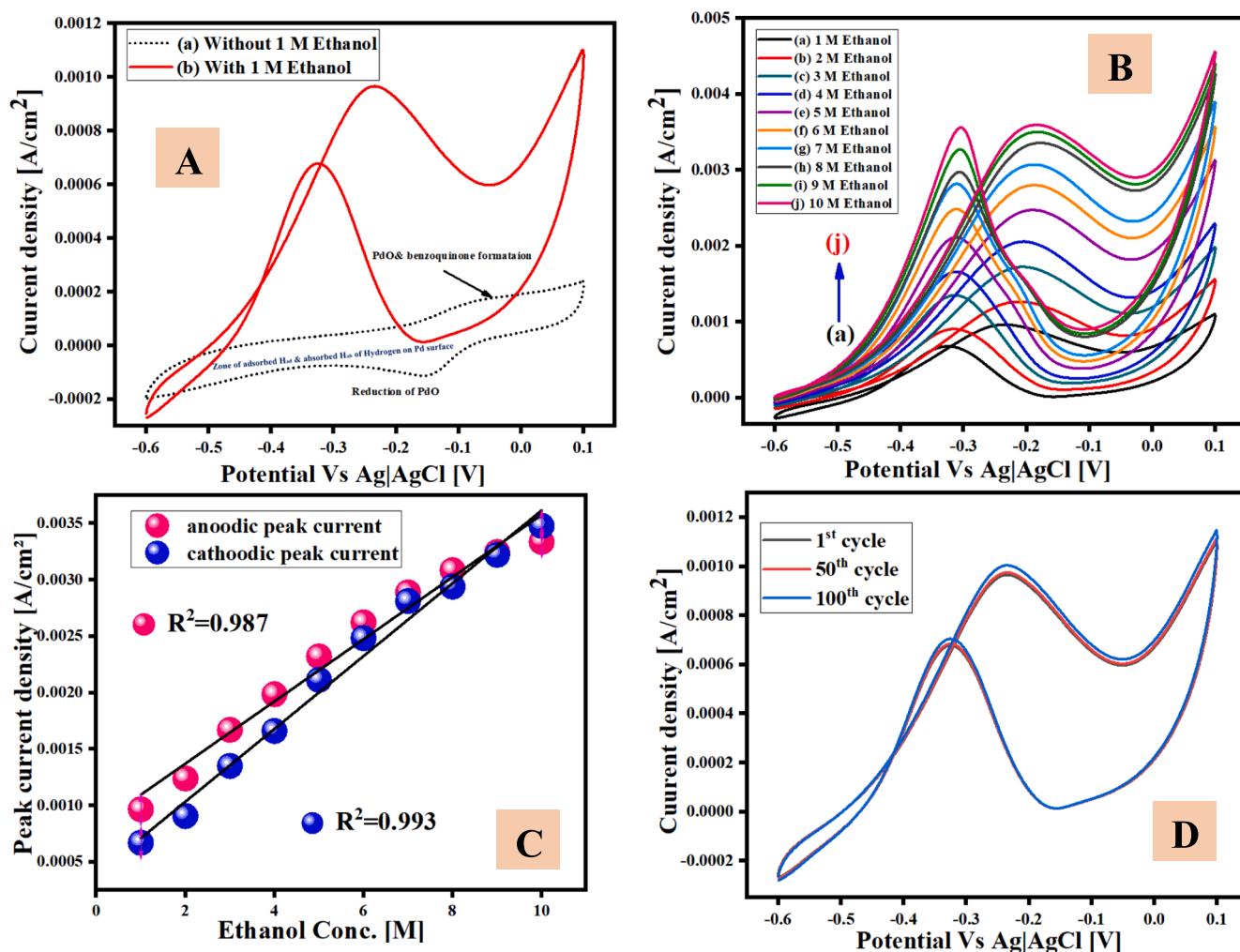
Fig. 8. CV of PI/Au-PAN/Pd flexible electrodes (A) (a) absence and (b) presence of 1 M ethanol at a sweep rate of 100 mV s^{-1}, (B) CV peaks of different concentrations from 1 to 10 M of ethanol, (C) anodic and cathodic peaks of various molar concentrations, and (D) stability analysis for 1 M ethanol at 1st and 100th cycles. All at an electrolyte background of 1 M KOH solution.

to its good electronegativity, the flexibility of the electrode, and one-step electrocatalyst fabrication this could find a potential usage in the energy sector.

Overall, the flexible, multifunctional PI/Au-PAN/Pd nanocomposite material delivers an extensive network of conducting pathways with more electroactive spots and it also offers high ionic diffusion that effortlessly facilitates the non-enzymatic electrochemical oxidation of glucose and the direct alcohol (methanol and ethanol) electrooxidation. The strong and synergistic metal-polymer interaction (MPI) between the conducting PAN and Pd suggests that these multifunctional flexible nanocomposite electrodes have extensive applications such as catalysts, efficient energy storage, and conversion material, and sensors for the future generation of multifunctional devices.

4. Conclusion

A flexible, multifunctional PI/Au-PAN/Pd nanocomposite material was fabricated to investigate the electrocatalytic performance of glucose, methanol, and ethanol. Physicochemical and electrochemical characterization authenticates the successful fabrication of semi-crystalline PAN NFs decorated Pd NPs over PI/Au surface. PI/Au-PAN/Pd nanocomposite material displayed ultra-high sensing performance towards glucose with a sensitivity of ~ 2140 µA/µM.cm^2 and a low LOD of ~ 0.3 µM (S/N = 3) with fast response time in ~ 2 s. Anti-

interference, reproducibility, and good stability of electrode claim its practical usage. Also, the efficient electrooxidation of methanol and ethanol with good stability was demonstrated by the flexible electrode. High electrocatalytic performance with excellent electron transfer pathway of PI/Au-PAN/Pd is notable, which is augmented due to the large accessible electroactive surface area with high ionic diffusion, and synergistic interaction between the Pd metal ions and the PAN NFs network structure. Hence, due to the versatile performance of this multifunctional electrode and it could be a promising electrocatalytic material for biosensor devices, and can be used as a single platform to oxidize glucose, methanol, and ethanol even at very low concentrations. Further, via the integration of the sensor and energy conversion system, and functionalization of this electroactive material finds potential applications in wearable healthcare diagnostics as well as alternative energy fields.

CRediT authorship contribution statement

Muthusankar Eswaran: Conceptualization, Methodology, Investigation, Writing – review & editing, Writing – original draft. **Shadi Rahimi:** Conceptualization, Writing – review & editing, Validation. **Santosh Pandit:** Conceptualization, Writing – review & editing, Validation. **Bavatharani Chokkiah:** Conceptualization, Writing – review & editing, Validation. **Ivan Mijakovic:** Supervision, Funding acquisition,

Resources.

Declaration of Competing Interest

The authors declare that they have no known competing financial interests or personal relationships that could have appeared to influence the work reported in this paper.

Data availability

The data that has been used is confidential.

Acknowledgments

Appendix A. Supplementary data

Supplementary data to this article can be found online at https://doi.org/10.1016/j.fuel.2023.128182.

References

[1] Yuan F, Xia Y, Lu Q, Xu Q, Shu Y, Hu X. Recent advances in inorganic functional nanomaterials based flexible electrochemical sensors. Talanta 2022;244:123419.

[2] Fang C, Zhong C, Chen N, Yi L, Li J, Weihua Hu. Reusable OIRD Microarray Chips Based on a Bienzyme-Immobilized Polyaniline Nanowire Forest for Multiplexed Detection of Biological Small Molecules. Anal Chem 2021;93(30):10697–703.

[3] Yoon J, Lee SN, Shin MK, Kim H-W, Choi HK, Lee T, et al. Flexible electrochemical glucose biosensor based on GOx/gold/MoS2/gold nanofilm on the polymer electrode. Biosens Bioelectron 2019;140:111343.

[4] Zhao P, Tang Q, Zhao X, Tong Y, Liu Y. Highly stable and flexible transparent conductive polymer electrode patterns for large-scale organic transistors. J Colloid Interface Sci 2018;520:58–63.

[5] Yang Y, Yang X, Zou X, Shiting Wu, Wan Da, Cao A, et al. Ultrafine graphene nanomesh with large on/off ratio for high-performance flexible biosensors. Adv Funct Mater 2017;27(19):1604096.

[6] Eswaran, Muthusankar, Pei-Chien Tsai, Ming-Tsang Wu, Vinoth Kumar Ponnusamy. Novel nano-engineered environmental sensor based on polymelamine/graphitic-carbon nitride nanohybrid material for sensitive and simultaneous monitoring of toxic heavy metals. J. Hazard. Mater. 2021;418:126267.

[7] Ma J, Liuxue Shen Yu, Jiang HM, Lv F, Liu J, Yan Su, et al. Wearable Self-Powered Smart Sensors for Portable Nutrition Monitoring. Anal Chem 2022;94(4):2333–40.

[8] Chokkiah B, Eswaran M, Wabaidur SM, Alothman ZA. Soo Chool Lee, Ragupathy Dhanusuraman. An efficient amperometric sensor for chloride ion detection through electroactive e-spun PVA-PANi-g-C3N4 nanofiber. J Mater Sci: Mater Electron 2022;33(12):9425–37.

[9] Phetsang S, Kidkhunthod P, Chanlek N, Jakmunee J, Mungkornasawakul P, Ounnunkad K. Copper/reduced graphene oxide film modified electrode for non-enzymatic glucose sensing application. Sci rep 2021;11:1–13.

[10] Muthusankar E, Wabaidur SM, Alothman ZA, Johan MR, Ponnusamy VK, Ragupathy D. Fabrication of amperometric sensor for glucose detection based on phosphotungstic acid–assisted PDPA/ZnO nanohybrid composite. Ionics 2020;26(12):6341–9.

[11] Eswaran M, Wabaidur SM, Alothman ZA, Dhanusuraman R, Ponnusamy VK. Ragupathy Dhanusuraman, Vinoth Kumar Ponnusamy. Improved cyclic retention and high-performance supercapacitive behavior of poly (diphenylamine-co-aniline)/phosphotungstic acid nanohybrid electrode. Int J Energy Res 2021;45(6):8180–8.

[12] Le QB, Nguyen T-H, Fei H, Bubulinca C, Munster L, Bugarova N, et al. "Electrochemical performance of composite electrodes based on rGO, Mn/Cu metal–organic frameworks, and PANI. Sci Rep 2022;12(1).

[13] Bavatharani C, Muthusankar E, Lee SC, Johan MR, Ragupathy D. Excellent cyclic retention and supercapacitive performance of electrochemically active nanocomposite electrode. Sens Lett 2020;18(5):395–400.

[14] Elancheziyan M, Eswaran M, Shuck CE, Senthilkumar S, Elumalai S, Dhanusuraman R, et al. Satheeshkumar Elumalai, Ragupathy Dhanusuraman, Vinoth Kumar Ponnusamy. Facile synthesis of polyaniline/titanium carbide (MXene) nanosheets/palladium nanocomposite for efficient electrocatalytic oxidation of methanol for fuel cell application. Fuel 2021;303:121329.

[15] Zhao L, Wen M, Fang H, Meng K, Qiu X, Wu Q, et al. NiCoPd Inlaid NiCo-Bimetallene for Efficient Electrocatalytic Methanol Oxidation. Inorg Chem 2022;61(26):10211–9.

[16] Chokkiah B, Eswaran M, Alothman AA, Alsawat M, Ifseisi AA, Alqahtani KN, et al. Facile fabrication of hollow polyaniline/carbon nanofibers-coated platinum nanohybrid composite electrode as improved anode electrocatalyst for methanol oxidation. J Mater Sci: Mater Electron 2022;33(11):8768–76.

[17] El-Refaei SM, Saleh MM, Awad MI. Enhanced glucose electrooxidation at a binary catalyst of manganese and nickel oxides modified glassy carbon electrode. J Power Sources 2013;223:125–8.

[18] Lin KC, Hung YT, Chen SM. Facile preparation of a highly sensitive nonenzymatic glucose sensor based on multiwalled carbon nanotubes decorated with electrodeposited metals. RSC Adv 2015;5:2806–12.

[19] Xu J, Cai J, Wang J, Zhang L, Fan Y, Zhang N, et al. Facile synthesis of hierarchically porous Co3O4 nanowire arrays with enhanced electrochemical catalysis. Electrochem Commun 2012;25:119–23.

[20] Li W, Ouyang R, Zhang W, Zhou S, Yang Y, Ji Y, et al. Single walled carbon nanotube sandwiched Ni-Ag hybrid nanoparticle layers for the extraordinary electrocatalysis toward glucose oxidation. Electrochim Acta 2016;188:197–209.

[21] Li S-J, Xia N, Lv X-L, Zhao M-M, Yuan B-Q, Pang H. A facile one-step electrochemical synthesis of graphene/NiO nanocomposites as efficient electrocatalyst for glucose and methanol. Sens Actuators B Chem 2014;190:809–17.

[22] Chokkiah B, Eswaran M, Wabaidur SM, Khan MR, Ponnusamy VK, Ragupathy D. A novel electrodeposited poly(melamine)-palladium nanohybrid catalyst on GCE: Prosperous multi-functional electrode towards methanol and ethanol oxidation. Fuel 2021;300:121005.

[23] Yu EH, Wang X, Krewer U, Li L, Scott K. Direct oxidation alkaline fuel cells: from materials to systems. Energy Environ Sci 2012;5:5668–80.

[24] Yang L, Tang Y, Yan D, Liu T, Liu C, Luo S. Polyaniline-reduced graphene oxide hybrid nanosheets with nearly vertical orientation anchoring palladium nanoparticles for highly active and stable electrocatalysis. ACS Appl Mater Interfaces 2016;8(1):169–76.

[25] Athawale AA, Bhagwat SV, Katre PP. Nanocomposite of Pd–polyaniline as a selective methanol sensor. Sens Actuators B Chem 2006;114(1):263–7.

[26] Prodromidis MI, Zahran EM, Tzakos AG, Bachas LG. Preorganized composite material of polyaniline–palladium nanoparticles with high electrocatalytic activity to methanol and ethanol oxidation. Int J Hydrogen Energy 2015;40(21):6745–53.

[27] Soleimani-Lashkenari M, Rezaei S, Fallah J, Rostami H. Electrocatalytic performance of Pd/PANI/TiO₂ nanocomposites for methanol electrooxidation in alkaline media. Synth Metals 2018;235:71–9.

[28] Eswaran M, Dhanusuraman R, Tsai P-C, Ponnusamy VK. Vinoth Kumar Ponnusamy. One-step preparation of graphitic carbon nitride/Polyaniline/Palladium nanoparticles based nanohybrid composite modified electrode for efficient methanol electro-oxidation. Fuel 2019;251:91–7.

[29] Ye J-S, Chen C-W, Lee C-L. Pd nanocube as non-enzymatic glucose sensor. Sens Actuators B Chem 2015;208:569–74.

[30] Rabti A, Argoubi W, Raouafi N. Enzymatic sensing of glucose in artificial saliva using a flat electrode consisting of a nanocomposite prepared from reduced graphene oxide, chitosan, nafion and glucose oxidase. Microchim Acta 2016;183(3):1227–33.

[31] Osuna, Velia, Alejandro Vega-Rios, Erasto Armando Zaragoza-Contreras, Iván Alziri Estrada-Moreno, Rocio B. Dominguez. Progress of polyaniline glucose sensors for diabetes mellitus management utilizing enzymatic and non-enzymatic detection. Biosensors2022;12(3): 137.

[32] Zhang Y, Liu J, Zhang Y, Liu J, Duan Y. Facile synthesis of hierarchical nanocomposites of aligned polyaniline nanorods on reduced graphene oxide nanosheets for microwave absorbing materials. RSC adv 2017;7(85):54031–8.

[33] Cantatore, Valentina, Santosh Pandit, V. R. S. S. Mokkapati, Severin Schindler, Siegfried Eigler, Ivan Mijakovic, Itai Panas. Design strategy of a graphene based bio-sensor for glucose. Carbon 2018;137: 343-348.

[34] Esquivel JP, Del Campo FJ, Gómez De La Fuente JL, Rojas S, Sabate N. Microfluidic fuel cells on paper: meeting the power needs of next generation lateral flow devices. Energy Environ Sci 2014;7(5):1744–9.

[35] Wang Y, Kwok HYH, Zhang Y, Pan W, Zhang H, Lu Xu, et al. A flexible paper-based hydrogen fuel cell for small power applications. Int J Hydrogen Energy 2019;44(56):29680–91.

[36] Carneiro LPT, Pinto AM, Goreti M, Sales F. Development of an innovative flexible paper-based methanol fuel cell (PB-DMFC) sensing platform–Application to sarcosine detection. J Chem Eng 2023;452:139563.

[37] Arun RK, Halder S, Chanda N, Chakraborty S. A paper based self-pumping and self-breathing fuel cell using pencil stroked graphite electrodes. Lab Chip 2014;14(10):1661–4.

[38] Chandra S, Lal S, Janardhanan VM, Sahu KC, Deepa M. Ethanol based fuel cell on paper support. J Power Sources 2018;396:725–33.

[39] Lal S, Janardhanan VM, Deepa M, Sagar A, Sahu KC. Low Cost Environmentally Benign Porous Paper Based Fuel Cells for Micro-Nano Systems. J Electrochem Soc 2015;162(14):F1402–7.

[40] Jiang Y, Liu H, Qi X, Sun J, Li M, Wang J. Conductive Ag-Based Modification of Hydroxyapatite Microtubule Array and Its Application to Enzyme-Free Glucose Sensing. ChemistrySelect 2018;3(9):2542–7.

[41] Ferhat-Hamida Z, Jr JB, Labruquere S, Duprez D. The chemical state of palladium in alkene and acetylene oxidation: A study by XRD, electron microscopy and TD-DTG analysis. Appl Catal B 2001;29(3):195–205.

[42] Zhang M, Liu Y, Wang J, Tang J. Photodeposition of palladium nanoparticles on a porous gallium nitride electrode for nonenzymatic electrochemical sensing of glucose. Microchim Acta 2019;186(2):1–8.